

**Rydberg-to- $M$ -shell x-ray emission of hollow  $\text{Xe}^{q+}$  ( $q = 27\text{--}30$ ) atoms or ions above metallic surfaces**Z. Y. Song (宋张勇),<sup>1</sup> Z. H. Yang (杨治虎),<sup>1,\*</sup> H. Q. Zhang (张红强),<sup>2</sup> J. X. Shao (邵剑雄),<sup>2</sup> Y. Cui (崔莹),<sup>2</sup> Y. P. Zhang (张艳萍),<sup>1,†</sup> X. A. Zhang (张小安),<sup>3</sup> Y. T. Zhao (赵永涛),<sup>1</sup> X. M. Chen (陈熙萌),<sup>2</sup> and G. Q. Xiao (肖国青)<sup>1</sup><sup>1</sup>*Institute of Modern Physics, Chinese Academy of Sciences, Lanzhou 730000, China*<sup>2</sup>*School of Nuclear Science and Technology, Lanzhou University, Lanzhou 730000, China*<sup>3</sup>*School of Physics and Electronic Engineering, Xianyang Normal University, Xianyang 712000, China*

(Received 23 October 2014; revised manuscript received 6 January 2015; published 21 April 2015)

X rays originating from transitions from high Rydberg states to the  $M$  shell (here called Rydberg-to- $M$ -shell x rays) have been measured in the interaction of  $\text{Xe}^{q+}$  ( $q = 27\text{--}30$ ) ions with aluminum, molybdenum, and beryllium surfaces in the energy range of 350–600 keV, by using a Si(Li) detector. The transition energy calculation by Cowan's program with relativistic correlation indicates that such x rays are mainly from the transition of the higher quantum states, with the principal quantum number from 6 up to 30, directly to  $M$  shell of xenon. The yield of the x ray per vacancy in  $M$  shell decreases slightly with increasing the projectile energies and is inversely proportional to the work functions of metallic surfaces used. However, it increases rapidly with the increase of the projectile charge states. All of these experimental facts combined with the transition rate calculations indicate that the measured Rydberg-to- $M$ -shell x rays come from the “above the surface” hollow Xe atoms or ions deexcitation, when the inner shells such as  $N$  and  $O$  have not been filled.

DOI: [10.1103/PhysRevA.91.042707](https://doi.org/10.1103/PhysRevA.91.042707)

PACS number(s): 34.35.+a, 32.30.Rj, 79.20.Rf

**I. INTRODUCTION**

A highly charged ion (HCI) has a large potential energy, which is equal to the binding energies of all the electrons removed to create the ion. When such a slow HCI approaches and then enters into a solid surface, an “above the surface” and a “below the surface” hollow atom will be formed, respectively, by capturing electrons from the surface into its empty levels [1–4]. Not only are new aspects of atom physics introduced by hollow atoms, but also HCI applications in material science provide promising prospects, such as surface analysis, the synthesis of materials with new properties, and the formation of nanostructures that have been an active area of research in recent years [5–8].

In order to obtain detailed understanding of the exotic hollow atom, the x-ray spectra [9–21] and the Auger electron spectra [22–29] during its formation and decaying have been investigated intensively over the past 20 years by several groups. Up to now reasonable agreement has been obtained regarding the formation of hollow atoms in the HCI surface interaction [30,31]. However, a lot of discussion is still going on regarding its decaying and the potential energy deposition [32–35], especially for the case of heavy ( $Z > 50$ ) highly charged ions colliding. After the HCI entering into the solid, for example, Watanabe *et al.* [10] measured the x-ray spectra with a Si(Li) detector as  $\text{I}^{q+}$  ( $q = 34\text{--}53$ ) ions impact on an H-terminated Si (Si-H) target surface. They found that the  $K$ -shell vacancies of hollow I atom were filled by x-ray emission with a probability of about 100% and the  $L$  vacancies with a probability of about 20%. Due to the fact that only a few of  $M$ -shell x rays were observed, they concluded that the decaying of the  $M$  vacancies were filled almost exclusively through Auger electron emission. Sun *et al.* [12] further found

that the  $L$  x-ray yield of hollow  $\text{I}^{q+}$  ions or atoms is related to the target material. Recently, Briand [20] and Pesic *et al.* [21] found much longer decay times of hollow atoms in dielectrics than in metals, and a significant decrease for the mean decay depth of hollow atoms with increasing projectile charge state. These findings indicate that the electronic property of the surface affects the formation and decaying mechanism of “below the surface” hollow atoms that, in turn, will further affect nanostructure formation.

Above the surface, electrons in highly excited states deexcite mainly through higher-rate multistep Auger [28,29] and lower-rate x-ray emission processes [1,13–16]. Since the Auger processes take many steps, thus a long time to decay to the inner shells, and the x-ray transition rate is roughly scaled with the square of energy difference between initial and final states  $\Delta E^2$ , it is possible to observe “above the surface” x-ray emission decaying directly from Rydberg states to the innermost shells. Such x rays are the fingerprints of the highly excited Rydberg atoms or ions.

In the present work,  $\text{Xe}^{q+}$  ( $q = 25\text{--}30$ ) ions with energy range from 350 to 600 keV were used to collide with several metallic surfaces and x-ray emission was observed by using a Si(Li) detector. With the aid of transition energy calculations we found that such x rays originate from the transitions of high Rydberg states with  $n$  ranging from 6 up to 30 directly to the  $M$  shell. The emphasis in this work is on the “above the surface” emission for such Rydberg-to- $M$ -shell x rays. In particular, we find a rapid increase of the x-ray yield with increasing projectile charge state. The dependence of the x-ray yield on the work functions of metallic surfaces (Al, Mo, Be) is also discussed.

**II. EXPERIMENTAL APPARATUS**

The experiment was carried out at the ECR ion source at the National Laboratory of the Heavy Ion Research Facility in Lanzhou. The details of the 14.5-GHz ECR ion source [36] and of the experimental setup [37,38] are described elsewhere.

\*z.yang@impcas.ac.cn

†Present address: College of Materials Science and Opto-electronic Technology, University of Chinese Academy of Sciences, Beijing 100049, China.

$\text{Xe}^{q+}$  ( $q = 25\text{--}30$ ) ions were extracted and selected by a  $90^\circ$  analyzing magnet. The beam passed through two apertures, 5 and 2 mm in diameter, and the beam spot on the target, placed at  $45^\circ$  with respect to the beam and polished with a purity of 99.99%, was about 2 mm. The base pressure in the chamber was maintained at about  $2 \times 10^{-8}$  mbar. The emitted x rays were transmitted through a beryllium window with a thickness of  $50 \mu\text{m}$  and were detected by a Si(Li) detector, placed at  $90^\circ$  to the beam, outside the chamber. The detector had a solid angle of 5.5 msr and an energy resolution of about 195 eV at 5.9 keV. For avoiding the interference of low energy x rays below 1.25 keV, a lower threshold was set in present experiments. To provide a count of the number of HCI, which impact on the surface during the x ray measurements, the target current was measured using a digital current integrator (ORTEC model 439) combined with a timer and counter (ORTEC model 871). Then the x-ray yield per ion was obtained from the x-ray counts and the ion counts.

### III. RESULTS AND DISCUSSION

Figure 1 shows the x-ray spectra observed as 450 keV  $\text{Xe}^{q+}$  ( $q = 25\text{--}30$ ) ions impinging on Al surface. The x-ray intensity is normalized to  $10^{13}$  incident projectiles and to the energy width corresponding to one channel of the MCA. The x-ray energy was calibrated by using the emitted x-ray lines from radioisotopes of  $^{241}\text{Am}$  and  $^{55}\text{Fe}$ . As can be seen from Figs. 1(a) and 1(b), the spectra consists of lower-intensity background x rays centered at about 1.75 keV, which primarily

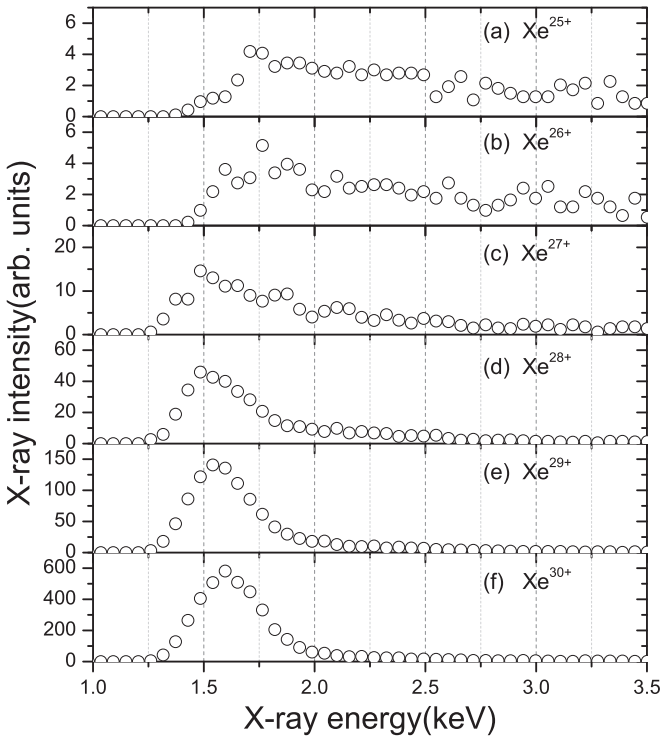


FIG. 1. X-ray spectra emitted in the interaction of 450 keV  $\text{Xe}^{q+}$  ( $q = 25\text{--}30$ ) ions with Al surface. For initial charge state  $q = 25$  and 26 only lower-intensity backgrounds primarily from Si escape x rays are observed, and for  $q = 27\text{--}30$  higher-intensity Rydberg-to- $M$ -shell x rays are observed as well as shifts in energies.

come from the Si escape x rays. However, the spectra resulting from  $\text{Xe}^{27+}$  to  $\text{Xe}^{30+}$  initial projectiles [Figs. 1(c) to 1(f)] show higher-intensity x rays with energies ranging from 1.3 to 2.0 keV. We note that the x-ray intensity increases rapidly and the x-ray energy position shifts toward higher energy with the increase of the projectile charge state  $q$ , i.e., with the number of initial  $M$ -shell vacancies. Maybe Al  $K$  x rays, induced by charge or vacancy transfer through radial coupling of  $3d\sigma$  and  $4f\sigma$  (correlated with Xe  $3d$  level and Al  $1s$  level, respectively) molecular orbitals in close collisions [23,39], have minor contributions to these peaks; however, they cannot be resolved due to limited energy resolution of our Si(Li) detector. From these figures we can also deduce that no additional  $L$ -shell vacancies are produced during the impact of  $\text{Xe}^{q+}$  ions on surfaces.

Machicoane *et al.* [14] measured  $M$ -shell x-ray spectra of  $\text{Xe}^{26+}$  (with no  $M$  vacancy) and  $\text{Xe}^{27+}$  (with one  $M$  vacancy) ions impact on Si surface using an IGLET-X windowless germanium detector for investigating the internal dielectronic excitation (IDE) [15]. In their work the measured spectra consist of two groups of x rays, a higher-intensity group with a central energy of about 780 eV and a lower-intensity one decaying monotonically from 0.9 to 1.5 keV. X rays with energies lower than 1.25 keV cannot be detected in present work because it is out of the sensitive range of the detector. Thus, no evidence can be observed for the IDE process because this mechanism takes place at an early stage of the hollow atom decaying and subsequently emitting a  $N$ - $M$  transition x ray with the energy of 0.8 keV.

According to the classical over-barrier model (COB) [30,31], as a  $\text{Xe}^{30+}$  ion approaches a critical distance  $R = \sqrt{2q}/W \approx 49$  a.u. from an Al surface with the work function  $W$  of 4.28 eV, it begins to resonantly capture conduction electrons into high Rydberg states (principal quantum number around  $n \approx 20\text{--}30$ ). Thus, an “above the surface” hollow Xe atom will be formed with electrons in higher orbitals and vacancies in inner shells. Usually the lifetime of the hollow Xe atom is longer than its approaching time (here  $\tau \approx 5$  fs) above the surface. Upon its impact on the surface, electrons in higher orbitals would be peeled off and, a more compact “below the surface” hollow atom will be formed after the projectile penetrates the surface. In addition to the primary multistep Auger deexcitation above the surface, electrons in highly excited states can also decay through a minor x-ray radiative process to the ground state, either directly or via a cascade. Below the surface, the inner-shell vacancies of the hollow Xe atom quickly decay on a time scale of femtoseconds [40,41] through  $M$ -shell x rays and Auger electrons emission.

In order to determine the origin of the observed x-ray spectra, energies and rates of transitions  $\Phi_0(N)\Phi_n(V) - 3d^{1-V}\Phi_0(N)$  (i.e.,  $nf\text{-}3d$ ) were calculated with Cowan’s program [42] for each charge state corresponding to the number  $V$  of  $M$ -shell vacancies from 1 to 4. Here  $\Phi_0(N) = 1s^2 2s^2 2p^6 3s^2 3p^6 3d^{10} 4s^{k_1} 4p^{k_2} 4d^{k_3} 5s^{k_4} 5p^{k_5}$ , the value of electron occupation number in outer shell ( $n \geq 4$ )  $N = k_1 + k_2 + k_3 + k_4 + k_5$  is from 0 to 26,  $\Phi_n(V) = 3d^{1-V}nf$ , the initial principal quantum number  $n$  is from 4 to 30. The calculated results were summarized in Table I, where the x-ray energy is the difference between the initial and

TABLE I. Calculated transition energies (eV) and weighted transition rates gA ( $s^{-1}$ ) of  $\Phi_0(N)\Phi_n(V) - 3d^{1-V}\Phi_0(N)$  using Cowan's program for each charge state  $q$  of  $Xe^{q+}$  ions.  $\Phi_0(N) = 1s^2 2s^2 2p^6 3s^2 3p^6 3d^{10} 4s^{k_1} 4p^{k_2} 4d^{k_3} 5s^{k_4} 5p^{k_5}$ ,  $N = k_1 + k_2 + k_3 + k_4 + k_5 = 0-26$  (values for  $N = 0, 8, 18,$  and  $26$  are listed),  $\Phi_n(V) = 3d^{-V}nf$ ,  $V = 1-4$ ,  $n = 4-30$ . For each charge state and each occupation number  $N$ , the first row lists the transition energies and the second is the corresponding weighted rates. The number in square brackets indicates the power of 10.

$q(V)$	$N$	$4f-3d$	$5f-3d$	$6f-3d$	$7f-3d$	$8f-3d$	$9f-3d$	$10f-3d$	$15f-3d$	$20f-3d$	$30f-3d$
27(1)	0	849	1085	1214	1291	1341	1375	1399	1456	1475	1489
		2.2[14]	9.8[13]	5.2[13]	3.1[13]	2.0[13]	1.3[13]	9.8[12]	2.7[12]	1.1[12]	3.3[11]
	8	779	923	996	1038	1065	1083	1096	1125	1135	1142
		1.3[14]	5.6[13]	3.0[13]	1.8[13]	1.2[13]	8.2[12]	5.8[12]	1.6[12]	6.8[11]	2.0[11]
	18	704	743	762	773	779	784	787	794	796	798
28(2)	0	882	1136	1274	1357	1410	1447	1473	1534	1555	1570
		2.2[15]	9.7[14]	5.1[14]	3.0[14]	1.9[14]	1.3[14]	9.5[13]	2.7[13]	1.1[13]	3.2[12]
	8	813	973	1054	1100	1130	1150	1164	1196	1207	1215
		1.4[15]	5.8[14]	3.1[14]	1.8[14]	1.2[14]	8.2[13]	5.9[13]	1.6[13]	6.9[12]	2.0[12]
	18	738	790	813	826	835	840	844	853	856	858
29(3)	0	915	1188	1335	1424	1481	1520	1548	1613	1636	1652
		9.8[15]	4.2[15]	2.2[15]	1.3[15]	8.4[14]	5.7[14]	4.1[14]	1.1[14]	4.8[13]	1.4[13]
	8	847	1024	1112	1163	1196	1218	1234	1270	1282	1290
		6.7[15]	2.6[15]	1.3[15]	8.3[14]	5.3[14]	3.6[14]	2.6[14]	7.4[13]	3.0[13]	8.9[12]
	18	772	837	866	882	892	898	903	914	917	920
30(4)	0	948	1240	1398	1492	1553	1595	1625	1695	1719	1736
		2.5[16]	1.0[16]	5.5[15]	3.2[15]	2.1[15]	1.4[15]	1.0[15]	2.8[14]	1.1[14]	3.5[13]
	8	880	1075	1171	1227	1263	1287	1304	1344	1357	1367
		1.7[16]	6.8[15]	3.6[15]	2.1[15]	1.3[15]	9.4[14]	6.7[14]	1.9[14]	7.8[13]	2.2[13]
	18	805	885	919	938	950	958	964	976	980	983
	26	797	828	834	836	838	839	840	841	842	842
		7.5[15]	3.1[14]	1.7[14]	1.0[14]	6.5[13]	4.4[13]	3.1[13]	8.3[12]	3.3[12]	9.4[11]

the final configuration-average energy, and the corresponding transition rate is the sum of weighted rates for all of allowed electric dipole transitions from the initial to the final states. For each charge state and each occupation number  $N$ , the first row lists the x-ray energies and the second corresponds to the weighted rates.

It should be noted that the electron capture from surface into high- $n$  shells occurs not only to the  $f$ -subshells but also into subshells with different angular momenta. Moreover, the populated states are strongly hybridized in front of the surface and atomic states with different angular momenta are mixed (Stark states) [43]. Therefore, it is very difficult in present work to evaluate how the captured electrons populate the different angular momentum subshells. Maybe a type of statistical angular momentum distribution would be expected. For comparison with  $nf-3d$  transitions, the transition rates gA of  $3d^{-1}np\Phi_0(0) - \Phi_0(0)$  ( $np-3d$ ) were also calculated and listed in Table II. The results indicates that the  $np-3d$  transition can be neglected as comparison with  $nf-3d$  transition. Table II also

includes the transition rates for  $3d^{-1}nd\Phi_0(0) - 3d^{-1}10f\Phi_0(0)$  ( $10f-nd$ ), which show that the electrons in highly states (here  $n = 10$ ) most like transitions into lower levels.

TABLE II. Calculated weighted rates gA ( $s^{-1}$ ) for all of allowed electric dipole transitions of  $3d^{-1}nd\Phi_0(0) - 3d^{-1}10f\Phi_0(0)$  and of  $3d^{-1}np\Phi_0(0) - \Phi_0(0)$ , respectively, with Cowan's program.  $\Phi_0 = 1s^2 2s^2 2p^6 3s^2 3p^6 3d^{10}$ ,  $n = 3-10$ . The number in square brackets indicates the power of 10.

Transitions	gA	Transitions	gA
$10f-3d$	9.8[12]	$4p-3d$	8.0[12]
$10f-4d$	2.6[13]	$5p-3d$	3.1[12]
$10f-5d$	1.1[13]	$6p-3d$	1.5[12]
$10f-6d$	5.4[12]	$7p-3d$	9.1[11]
$10f-7d$	2.8[12]	$8p-3d$	5.7[11]
$10f-8d$	1.4[12]	$9p-3d$	3.8[11]
$10f-9d$	6.5[11]	$10p-3d$	2.7[11]

As can be seen from Table I, while the  $N$  and  $O$  shells have fewer spectator electrons present at the time of x-ray emission, the calculated x-ray energies establish the peaks from 1.3 to 1.8 keV as filling the initial vacancies in  $M$  shell directly from highly excited states with principal quantum number ranging from 6 to 30, i.e., Rydberg-to- $M$ -shell x rays emission. It should be noted that the calculated x-ray energy range are smaller than the experimental results (1.3–2.0 keV). This could be explained by taking into account the upward shifts of the ionic energy levels since the interaction of the ion with its image charge as the ion approaches the metallic surface. Therefore, the observed x rays in Figs. 1(c) to 1(f) come from the “above the surface” hollow Xe atoms or ions deexcitation, while many of inner shell ( $N$  and  $O$  *et al.*) vacancies are not filled. On the contrary, the calculated results indicate the measured x rays peaked around 780 eV by Machicoane [see Ref. [14], Figs. 1(a) and 1(b)] mainly from the “below the surface” hollow atoms deexcitation. At that time the  $N$ ,  $O$  shells have been filled as  $\text{Xe}^{27+}$  ions penetrating surfaces, just leaving an empty  $M$  shell. Because the transition rates from  $nf$  ( $n \geq 6$ ) to  $3d$  level gradually decrease with increasing the principal quantum number  $n$ , an exponential decay spectrum shape would be expected other than the observed symmetrical shape as shown in Fig. 1. This is induced by two possible reasons. One is related to the electronic lower threshold of 1.25 keV set in measurements, and the other is to the surface oxidization and dissociative adsorption of hydrogen, yielding a coverage of hydrogen, carbon, and oxygen on the surface. As highly charged Xe ions approach the surface, in addition to the capture of conduction electrons to high states ( $n \approx 20$ –30), the binding electrons of neutral atoms adsorbed on the surface will, in addition, lead to capture into states with a principal quantum number around  $n_c \approx q^{3/4} \approx 11$ . Thus, the x-ray radiative rate from this orbital directly to the ground state should be larger than that from other states, even though  $n < n_c$ , yielding the x-ray spectra shape with a peak value corresponding nearly to this transition energy. It should be noted that, for  $\text{Xe}^{27+}$  ion incidence [Fig. 1(c)], the background due to Si escape x rays is considerable compared with the Rydberg-to- $M$ -shell x rays, and it accounts for the spectra larger than 1.5 keV. For  $\text{Xe}^{30+}$  the background takes a small amount and can be neglected.

From the measured x-ray counts, the x-ray yield can be obtained by taking into account the background, the solid angle of the detector seen from the target, the total number of incident particles, the detector efficiency, and the absorption of 0.8 cm air and a 50- $\mu\text{m}$  beryllium window. The incoming electrical beam current  $I_{\text{in}}$  was estimated from the measured target current  $I_t$  after correcting the secondary electron emission yield by using the equation  $I_{\text{in}} = I_t / (1 + \gamma/q)$ . By division of  $I_{\text{in}}$  by the charge of the projectile ion the incoming particle current is determined. Basing on the measured secondary electron yield in Refs. [24,25] for perpendicular incidence of Xenon ions on several metal surfaces and, taking into account the scattering geometry in present work, a value of  $\gamma/q$  is estimated with a error of 15% for calculating the x-ray yield and its error. For these energy range x rays, the detector efficiency of Si(Li) detector with a 25- $\mu\text{m}$  beryllium window was 38%, and the absorption for 0.8 cm air and a 50- $\mu\text{m}$  beryllium window was from 0.06 to 0.1 [44].

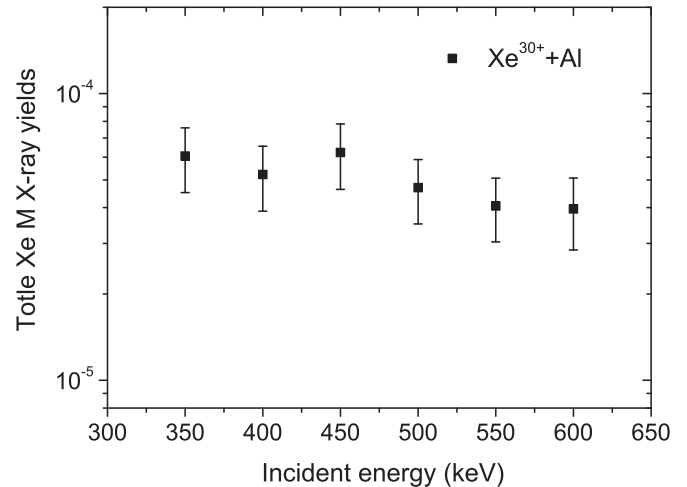


FIG. 2. Xe Rydberg-to- $M$ -shell x-ray yields following  $\text{Xe}^{30+}$  ions impact on Al surfaces as a function projectile energies from 350 to 600 keV.

Figure 2 shows the measured x-ray yields for  $\text{Xe}^{30+}$  ions impact on Al surface as a function of projectile energies from 350 to 600 keV. The error bars primarily result from uncertainties of the number of incident ions (15%), the observation solid angle (2%), the efficiency of x-ray detector (2%), and the x-ray counting statistics (10%), therefore the total uncertainty is about 30%. As shown in this figure the yield decreases slightly with the increasing of projectile energies. This result is another evidence that the measured x rays are from the “above the surface” hollow Xe atoms or ions deexcitation. Because such x-ray emission process will end as Xe atoms or ions arriving at the surface, the ions with lower velocity will have more time decaying than the ions with higher velocity, thus more x-ray yields would be expected. It should be noted that although the yield of such x rays decreases as increasing the projectile energies it is still within the experimental uncertainties. It also should be noted that such Rydberg-to- $M$ -shell x-ray emission occurred above the surface just allows for a very small fraction of the deexcitation of the  $M$ -shell holes. Most of the  $M$ -shell vacancies would be filled below the surface given more time, as pointed out in Ref. [21] that the  $M$ -shell holes of hollow lead atoms are primarily filled below the surface within 22–68 fs.

Figure 3 shows x-ray yields divided by the initial number of vacancies in  $M$  shell as a function of projectile charge states for  $\text{Xe}^{q+}$  ( $q = 27$ –30) ions impact on Al surface. As shown in this figure the yield increases rapidly as increasing the initial  $M$ -shell vacancies. It is not surprising because the x-ray emission in the present work occurs on the surface and only associates with the radiative transitions from highly excited states directly to the ground states. The radiative rates of such transitions increase around 100 times, as shown in Table I, as  $\text{Xe}^{q+}$  ions charge state increasing from 27 to 30. However, the x-ray yield per  $M$  hole measured by Machicoane *et al.* [14] should be constant with initial  $M$  vacancies, or should increase slightly because of the reduced screening of the core for higher charge states. This is because these x rays are emitted primarily below the surface where the  $N$ ,  $O$  shells have been filled due

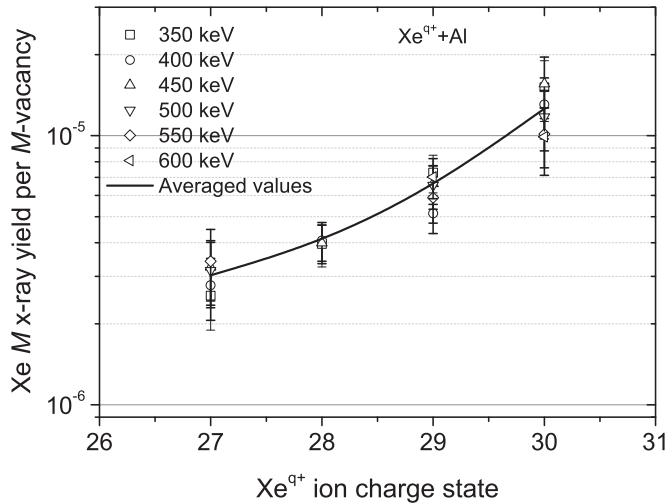


FIG. 3. Xe Rydberg-to-*M*-shell x-ray yields divided by the initial number of *M*-shell vacancies as a function of projectile charge states for  $\text{Xe}^{q+}$  ( $q = 27$ – $30$ ) ions impact on Al surfaces with incident energies  $\square$  350,  $\circ$  400,  $\triangle$  450,  $\nabla$  500,  $\diamond$  550, and  $\triangleleft$  600 keV, respectively. The B-spline line represents the arithmetic mean values over the yields induced by ions with different kinetic energies.

to these levels closing to the Fermi level of the metal surface. Thus, the measured x-ray yield is nearly equal to the *M*-shell fluorescence yield, which is likely to be proportional to the initial *M* vacancies. The approximately linear relationship of the *M* x-ray yield (or *M*-shell fluorescence yield) of  $\text{Bi}^{q+}$  ions impact on Au surface [3,16] with charge state from  $q = 56$  to  $q = 64$  also indicates that these x rays with energy ranging from 2.5 to 6.0 keV were emitted below the surface. As charge state  $q < 56$  lower-intensity x rays in this energy range were also observed. However, such x rays can not be used as the evidence for decaying directly from highly Rydberg states to the empty *N* shell. This is because the possible IDE mechanism and the molecular promotion process can induce

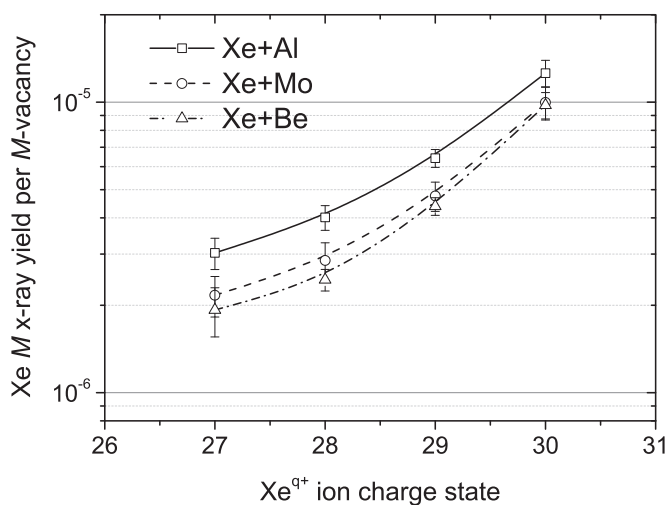


FIG. 4. Averaged Xe Rydberg-to-*M*-shell x-ray yields per *M*-shell vacancy as a function of projectile charge states for  $\text{Xe}^{q+}$  ( $q = 27$ – $30$ ) ions impact on Al, Mo, and Be surfaces.

TABLE III. The averaged Rydberg-to-*M*-shell x-ray yields over values induced by different projectile energies for individual charge state. Numbers in parentheses indicate power of ten.

	27	28	29	30
Al	3.03(−6)	4.01(−6)	6.42(−6)	12.6(−6)
Mo	2.17(−6)	2.85(−6)	4.76(−6)	9.99(−6)
Be	1.92(−6)	2.45(−6)	4.38(−6)	9.76(−6)

normal *M*-shell x rays, whose energies are superimposed with the Rydberg-to-*N*-shell x rays. In fact, the Rydberg-to-*M*- or -*N*-shell x rays primarily radiate above the surface and its transition rate is strongly related with the vacancy number in *M* or *N* shell of the hollow atom or ion.

A simple estimation of the Rydberg-to-*M*-shell x-ray yield  $Y_{\text{Ryd}}$  can be made basing on the equation  $Y_{\text{Ryd}} = P_{\text{cap}}[1 - \exp(-\bar{A}t)]$  with  $\bar{A}$  the mean transition rate from highly states to the ground state and,  $P_{\text{cap}}$  represents the electron capture probability from the surface. For  $\text{Xe}^{27+}$  and  $\text{Xe}^{30+}$  ions incidence, x-ray yield of  $0.05P_{\text{cap}}$  and  $0.99P_{\text{cap}}$  would be obtained, respectively, as substituting the decaying time of 5 fs, transition rate of  $0.01 \text{ fs}^{-1}$  for  $\text{Xe}^{27+}$  and  $1 \text{ fs}^{-1}$  for  $\text{Xe}^{30+}$  to the equation. This result is accordance approximately with the measured ratio of yields  $R \approx 17$  for  $\text{Xe}^{30+}$  to  $\text{Xe}^{27+}$ .

We also measured such Rydberg-to-*M*-shell x rays of  $\text{Xe}^{q+}$  ( $q = 27$ – $30$ ) ions colliding with Mo and Be surfaces in the same energy range. Also the x-ray yield is nearly a constant in the projectile energy range studied here for individual charge state; and the normalized yield by the number of initial *M* vacancies has expanded around four times as increasing the charge state from 27 to 30. However, the x-ray yield depends on target materials. As shown in Figs. 3 and 4 and Table III, the x-ray yield colliding with Al surface is larger than that with Mo surface, and the yield with Be surface is the minimum. Al *K* x rays induced by charge transfer process in close collisions have minor contributions (no more than 20%) to the measured spectra. However, the x-ray yield on Al surface is about 1.3–1.5 times larger than the yields on Mo and Be. In fact, this result indicates further that the measured Rydberg-to-*M*-shell x rays are due to the “above the surface” hollow atoms or ions deexcitation. As discussed above, the critical distance  $R$  from the ion to the surface is inversely proportional to the work function  $W$  of metallic surface. For Al, Mo, and Be materials the work function are 4.28, 4.6, and 4.98 eV, respectively, so the  $R$  from Al surface is maximum and from Be is minimum. It means that the electrons in Rydberg states captured from Al surfaces have the most time to decay compared with Mo and Be surfaces.

#### IV. CONCLUSIONS

In summary, we have investigated the x-ray emission in the interactions of  $\text{Xe}^{q+}$  ( $q = 25$ – $30$ ) ions with Al, Mo, and Be surfaces in the energy range of 350–600 keV. Rydberg-to-*M*-shell x-ray emission of Xenon was found when the projectiles have the initial *M*-shell vacancies and, equivalently, the charge state of incident Xenon ions is over 27. The calculated results by Cowan’s program with relativistic correlation indicate that such x rays are emitted as filling the initial *M* vacancies directly

from highly excited states with principal quantum number ranging from 6 to 30. We found that the x-ray yield per vacancy in  $M$  shell decreases slightly with the increase of incident energies and is inversely proportional to the work functions of surfaces used. However, it increases rapidly with the increase of the projectile charge states. This is in accordance with the calculation of the transition rates, which are strongly related with the initial number of vacancies in  $M$  shell of the Xenon ions or atoms. These experimental facts indicate that such x rays are emitted primarily above the surface, and at the time

of transitions there are fewer spectator electrons in  $N$ ,  $O$  shells present, i.e., these shells are not filled completely.

#### ACKNOWLEDGMENTS

This work is supported by National Natural Science Foundation of China (NSFC) (Grants No. 11005133 and No. 11174296). We thank the staff of ECR ion source for arrangement and operation of the ion source.

- 
- [1] J. P. Briand, L. de Billy, P. Charles, S. Essabaa, P. Briand, R. Geller, J. P. Desclaux, S. Bliman, and C. Ristori, *Phys. Rev. Lett.* **65**, 159 (1990).
- [2] F. W. Meyer, S. H. Overbury, C. C. Havener, P. A. Zeijlmans van Emmichoven, and D. M. Zehner, *Phys. Rev. Lett.* **67**, 723 (1991).
- [3] T. Schenkel, A. V. Hamza, A. V. Barnes, and D. H. Schneider, *Prog. Surf. Sci.* **61**, 23 (1999).
- [4] A. Arnau, F. Aumayr, P. M. Echenique, M. Grether, W. Heiland, J. Limburg, R. Morgenstern, P. Roncin, S. Schippers, R. Schuch, N. Stolterfoht, P. Varga, T. J. M. Zouros, and HP. Winter, *Surf. Sci. Rep.* **27**, 113 (1997).
- [5] E. Akcoeltek, T. Peters, R. Meyer, A. Duvenbeck, M. Klusmann, I. Monnet, H. Lebius, and M. Schleberger, *Nat. Nanotechnol.* **2**, 290 (2007).
- [6] R. Heller, S. Facsko, R. A. Wilhelm, and W. Möller, *Phys. Rev. Lett.* **101**, 096102 (2008).
- [7] A. S. El-Said, R. Heller, W. Meissl, R. Ritter, S. Facsko, C. Lemell, B. Solleder, I. C. Gebeshuber, G. Betz, M. Toulemonde, W. Möller, J. Burgdörfer, and F. Aumayr, *Phys. Rev. Lett.* **100**, 237601 (2008).
- [8] A. S. El-Said, R. A. Wilhelm, R. Heller, S. Facsko, C. Lemell, G. Wachter, J. Burgdörfer, R. Ritter, and F. Aumayr, *Phys. Rev. Lett.* **109**, 117602 (2012).
- [9] S. J. McMahon, A. P. Kavanagh, H. Watanabe, J. Sun, M. Tona, N. Nakamura, S. Ohtani, and F. J. Currell, *Phys. Rev. A* **83**, 022901 (2011).
- [10] H. Watanabe, S. Takahashi, M. Tona, N. Yoshiyasu, N. Nakamura, M. Sakurai, C. Yamada, and S. Ohtani, *Phys. Rev. A* **74**, 042901 (2006).
- [11] H. Watanabe, J. Sun, M. Tona, N. Nakamura, M. Sakurai, C. Yamada, N. Yoshiyasu, and S. Ohtani, *Phys. Rev. A* **75**, 062901 (2007).
- [12] J. Sun, H. Watanabe, M. Tona, T. Watanabe, N. Nakamura, C. Yamada, and S. Ohtani, *Phys. Rev. A* **77**, 032901 (2008).
- [13] J. P. Briand, S. Thuriez, G. Giardino, G. Borsoni, M. Froment, M. Eddrief, and C. Sebenne, *Phys. Rev. Lett.* **77**, 1452 (1996).
- [14] G. A. Machicoane, T. Schenkel, T. R. Niedermayr, M. W. Newmann, A. V. Hamza, A. V. Barnes, J. W. McDonald, J. A. Tanis, and D. H. Schneider, *Phys. Rev. A* **65**, 042903 (2002).
- [15] R. Schuch, D. Schneider, D. A. Knapp, D. DeWitt, J. McDonald, M. H. Chen, M. W. Clark, and R. E. Marrs, *Phys. Rev. Lett.* **70**, 1073 (1993).
- [16] M. W. Clark, D. H. Schneider, E. F. Deveney, Q. C. Kessel, E. Pollack, and W. W. Smith, *Nucl. Instrum. Meth. B* **79**, 183 (1993).
- [17] Z. Y. Song, Z. H. Yang, G. Q. Xiao, Q. M. Xu, J. Chen, B. Yang, and Z. R. Yang, *Eur. Phys. J. D* **64**, 197 (2011).
- [18] J. P. Briand, D. Schneider, S. Bardin, H. Khemliche, J. Jin, Z. Xie, and M. Prior, *Phys. Rev. A* **55**, 3947 (1997).
- [19] X. Zhang, Y. Zhao, H. H. Hoffmann, Z. Yang, X. Chen, Z. Xu, F. Li, and G. Xiao, *Laser Part. Beams* **29**, 265 (2011).
- [20] J. P. Briand, R. Phaneuf, N. B. Aryal, K. K. Baral, C. M. Thomas, and D. A. Esteves, *Phys. Rev. A* **88**, 034901 (2013).
- [21] Z. D. Pesic, Gy. Viktor, S. Atanassova, J. Anton, S. Leontein, M. Björkhage, A. Paál, H. Hanafy, and R. Schuch, *Phys. Rev. A* **75**, 012903 (2007).
- [22] H. Kurz, K. Töglhofer, H. P. Winter, F. Aumayr, and R. Mann, *Phys. Rev. Lett.* **69**, 1140 (1992).
- [23] S. Schippers, S. Hustedt, W. Heiland, R. Köhrbrück, J. Bleck-Neuhaus, J. Kemmler, D. Lecler, and N. Stolterfoht, *Phys. Rev. A* **46**, 4003 (1992).
- [24] F. Aumayr, H. Kurz, D. Schneider, M. A. Briere, J. W. McDonald, C. E. Cunningham, and H. P. Winter, *Phys. Rev. Lett.* **71**, 1943 (1993).
- [25] J. Krása, L. Láska, M. P. Stöckli, and C. W. Fehrenbach, *Nucl. Inst. Meth. Phys. B* **196**, 61 (2002).
- [26] G. Ruano, R. A. Vidal, J. Ferron, and R. A. Baragiola, *Surf. Sci.* **605**, 1807 (2011).
- [27] N. Bajales, L. Cristina, S. Mendoza, R. A. Baragiola, E. C. Goldberg, and J. Ferron, *Phys. Rev. Lett.* **100**, 227604 (2008).
- [28] N. Stolterfoht, A. Arnau, M. Grether, R. Köhrbrück, A. Spieler, R. Page, A. Saal, J. Thomaschewski, and J. Bleck-Neuhaus, *Phys. Rev. A* **52**, 445 (1995).
- [29] J. Limburg, S. Schippers, R. Hoekstra, R. Morgenstern, H. Kurz, F. Aumayr, and H. P. Winter, *Phys. Rev. Lett.* **75**, 217 (1995).
- [30] J. Burgdörfer, P. Lerner, and F. W. Meyer, *Phys. Rev. A* **44**, 5674 (1991).
- [31] J. J. Ducree, F. Casali, and U. Thumm, *Phys. Rev. A* **57**, 338 (1998).
- [32] T. Schenkel, A. V. Barnes, T. R. Niedermayr, M. Hattass, M. W. Newman, G. A. Machicoane, J. W. McDonald, A. V. Hamza, and D. H. Schneider, *Phys. Rev. Lett.* **83**, 4273 (1999).
- [33] U. Kentsch, H. Tyrroff, G. Zschornack, and W. Möller, *Phys. Rev. Lett.* **87**, 105504 (2001).
- [34] D. Kost, S. Facsko, W. Möller, R. Hellhammer, and N. Stolterfoht, *Phys. Rev. Lett.* **98**, 225503 (2007).
- [35] R. E. Lake, J. M. Pomeroy, H. Grube, and C. E. Sosolik, *Phys. Rev. Lett.* **107**, 063202 (2011).

- [36] L. T. Sun, J. Y. Li, X. Z. Zhang, H. Wang, B. H. Ma, X. X. Li, Y. C. Feng, M. T. Song, Y. H. Zhu, L. M. Zhao, P. Z. Wang, H. P. Liu, H. W. Zhao, X. W. Ma, and W. L. Zhan, *High Energy Phys. Nucl. Phys.* **31**(S1), 55 (2007).
- [37] X. M. Chen, J. X. Shao, Z. H. Yang, H. Q. Zhang, Y. Cui, X. Xu, G. Q. Xiao, Y. T. Zhao, X. A. Zhang, and Y. P. Zhang, *Eur. Phys. J. D* **41**, 281 (2007).
- [38] H. Zhang, X. Chen, Z. Yang, J. Xu, Y. Cui, J. Shao, X. Zhang, Y. Zhao, Y. Zhang, and G. Xiao, *Nucl. Instrum. Meth. B* **268**, 1564 (2010).
- [39] A. Arnau, R. Köhrbrück, M. Grether, A. Spieler, and N. Stolterfoht, *Phys. Rev. A* **51**, R3399 (1995).
- [40] M. Hattass, T. Schenkel, A. V. Hamza, A. V. Barnes, M. W. Newman, J. W. McDonald, T. R. Niedermayr, G. A. Machicoane, and D. H. Schneider, *Phys. Rev. Lett.* **82**, 4795 (1999).
- [41] S. Martin, R. Bredy, J. Bernard, J. Desesquelles, and L. Chen, *Phys. Rev. Lett.* **89**, 183401 (2002).
- [42] R. D. Cowan, *The Theory of Atomic Structure and Spectra* (The University of California Press, Oakland, 1985).
- [43] P. Kürpick and U. Thumm, *Phys. Rev. A* **58**, 2174 (1998).
- [44] J. H. Hubbell and S. M. Seltzer, <http://www.nist.gov/pml/data/xraycoef/>.